

Metal-insulator transition in low dimensional $\text{La}_{0.75}\text{Sr}_{0.25}\text{VO}_3$ thin films

Tran M. Dao,¹ Partha S. Mondal,¹ Y. Takamura,² E. Arenholz,³ and Jaichan Lee^{1*}

¹School of Advanced Materials Science and Engineering, Sungkyunkwan University, Suwon, 440-746, Korea.

²Department of Chemical Engineering and Materials Science, University of California, Davis, Davis, CA 95616, USA

³Advanced Light Source, Lawrence Berkeley Lab., Berkeley, CA 94720, USA

Abstract

We report on the metal-insulator transition that occurs as a function of film thickness in ultrathin $\text{La}_{0.75}\text{Sr}_{0.25}\text{VO}_3$ films. The metal-insulator transition displays a critical thickness of 5 unit cell. Above the critical thickness, metallic films exhibit a temperature driven metal-insulator transition with weak localization behavior. With decreasing film thickness, oxygen octahedron rotation in the films increases, causing enhanced electron-electron correlation. The electron-electron correlations in ultrathin films induce the transition from metal to insulator in addition to Anderson localization.

*Electronic mail : jclee@skku.edu.

The metal-insulator transition (MIT) in 3d transition metal oxides (TMO) has been attracting intensive attention in condense matter physics.¹ According to the Mott-Hubbard model, a MIT can be controlled by varying the relative magnitude of the on-site Coulomb repulsion and bandwidth even in a system without disorder. Whereas in the absence of Coulomb repulsion, only coherent backscattering of non-interacting electrons from the randomly distributed impurities can lead to Anderson localization of electrons and can drive the MIT.^{2,3} Hence the interplay between disorder and electronic correlation leads to subtle many-body effects and complicate the MIT phenomenon in TMOs.⁴

Lanthanum strontium vanadate ($\text{La}_{1-x}\text{Sr}_x\text{VO}_3$) is a canonical system for studying filling-controlled MIT.⁵⁻⁷ The parent compound LaVO_3 is an antiferromagnetic Mott insulator with strong electron-electron correlation. Upon Sr doping, the electrical transport characteristics gradually change from insulating to metallic with a MIT transition around $x=0.178$,⁷ while the end member SrVO_3 exhibits a robust metallic state. It is already established that the MIT can be influenced by Anderson localization due to disorder provided by the random distribution of Sr^{2+} and La^{3+} ions on the A site of the perovskite (ABO_3) structure.³ Close to the MIT, the metallic state of $\text{La}_{1-x}\text{Sr}_x\text{VO}_3$ can be changed by the carrier localization effect, perhaps due to poor shielding of the impurity (Sr^{2+}) potential by the low carrier density.⁵ Despite extensive studies on polycrystalline and single crystalline $\text{La}_{1-x}\text{Sr}_x\text{VO}_3$ bulks, few reports are available on thin films.⁵⁻
⁷ Lekshmi *et al*, studied filling-controlled MIT in $\text{La}_{1-x}\text{Sr}_x\text{VO}_3$ thin films.⁸ The MIT was observed in the region $0.175 < x < 0.2$, mirroring the results for bulk $\text{La}_{1-x}\text{Sr}_x\text{VO}_3$. In contrast, Yoshimatsu *et al*. reported bandwidth-controlled MIT in SrVO_3 ultrathin films. They observed a dimensional crossover in the absence of any chemical fluctuation or disorder, such that MIT occurred at a critical thickness between 2 and 3 unit cells (uc).⁹ In this study, we report the MIT

and associated driving mechanisms in ultrathin $\text{La}_{0.75}\text{Sr}_{0.25}\text{VO}_3$ (LSVO) films as a function of film thickness. At this nominal composition, bulk LSVO exhibits correlated metal behavior. However, the metallic state changed into an insulating state as the thickness of LSVO films was progressively reduced to 5 uc. This behavior was attributed to electron correlation and Anderson localization.

High-quality ultrathin LSVO epitaxial films with thickness ranging from 5 to 25 uc were deposited on atomically flat (r.m.s roughness $\sim 1.6\text{\AA}$) (001) oriented LaAlO_3 (LAO) substrate by pulsed laser deposition assisted by in-situ reflection high energy electron diffraction (RHEED). The unit cell thickness is defined the length of VO_6 octahedron. Polycrystalline $(\text{La}_{0.75}\text{Sr}_{0.25})_2\text{V}_2\text{O}_7$ was used as the target. Following the deposition of LSVO layer, 10nm thick LAO capping layer was deposited to prevent the oxidation of vanadium. All samples were grown at 600°C in an oxygen partial pressure 1×10^{-6} torr with a laser energy density of 1.5 J/cm^2 . RHEED patterns confirmed two dimensional layer-by-layer growth of the LSVO films.¹⁰ The film thickness was precisely controlled by monitoring the intensity oscillations of RHEED patterns. Single phase structure was confirmed by high resolution X-ray diffraction (XRD) using beamline 3C2 at Pohang Accelerator Light Source (PALS), Korea. Temperature dependent resistivity of the LSVO thin films was investigated using Van der Pauw method in a low temperature probe station with He-cryostat. The temperature was varied from range 4K to 400K, the bias current was $10 \mu\text{A}$, and the electrical contacts were made to photolithographically buried gold contacts. X-ray absorption spectroscopy (XAS) was performed on LSVO films with 3 uc thick LAO capping layer at beamline 4.0.2. at the Advance Light Source (ALS), USA. The $\text{V}2p$ and $\text{O}1s$ edges were recorded using the total electron yield method in normal and grazing incidence relative to the film surface.

The RHEED intensity oscillations during the growth of LSVO films are shown in Fig. 1. The inset figure shows the AFM topography image of LSVO film with 8 uc thickness deposited on LAO substrate. The LSVO films maintained good step-terrace structure with a step height of ~ 4 Å, indicating that the deposition was carried out in layer-by-layer growth mode and film thickness was precisely controlled. Figure 2(a) shows high resolution XRD patterns for the films with varying thickness, indicating that the films are single phase with a (001) orientation. The reciprocal space mapping (-103) of LSVO film with a thickness of 25 uc (Fig.2 (c)) indicates that the film exhibits fully coherent nature with the substrate. This suggests that the LSVO films thinner than 25 uc also show the coherent nature. Due to the lattice mismatch ($\sim 3\%$), the LSVO films are expected to experience an in-plane compressive strain from the underlying LAO substrate, resulting in an elongation of the out-of-plane (c-axis) lattice parameter compared to bulk value. However, as shown in Fig. 2(b), the c-axis lattice parameter increases as the film thickness increases up to 25 uc. On further increase of thickness it begins to decrease (not shown in the figure) and gradually approaches to the bulk value. This result clearly indicates the 25 uc thickness is the pseudomorphic limit or critical thickness for strain relaxation LSVO films on LAO substrate, above which the strain relaxation through the formation of misfit dislocations is expected to occur. Bulk LSVO exhibits an orthorhombic structure with GdFeO_3 -type distortions allowing for oxygen octahedron rotation.¹¹ In perovskite thin films, BO_6 oxygen octahedron rotation can occur to accommodate epitaxial strain.¹² Therefore, in the ultrathin LSVO films below 25 uc thickness, VO_6 octahedron rotation is a possible strain relaxation mechanism to accommodate the compressive strain, which is accompanied by the decrease of c-axis lattice parameter. The octahedron rotation gradually increases with decreasing film thickness, resulting in the gradual decrease in the c-axis lattice parameter with decreasing film thickness. The VO_6

octahedron rotation gives rise to a change in the V-O-V bond angle, which can result in the decrease in hybridization between V and oxygen ions (i.e. $V3d$ and $O2p$ states) and consequently a narrowing of the one electron bandwidth.

The resistivity as a function of temperature, $\rho(T)$, for LSVO films of varying thickness was measured in the temperature range 4-400K (Fig. 3). Around room temperature, the films with thickness larger than 8 μm showed metallic behavior ($d\rho/dT > 0$). On further reduction of the thickness, a thickness-driven MIT occurred between 5 and 8 μm thickness such that at 5 μm thickness, the electrical transport behavior changed to an insulating characteristic ($d\rho/dT < 0$) for entire temperature range studied. The metallic films exhibited a temperature-driven MIT (resistivity upturn at low temperature) with a characteristic temperature (T_{MI}). T_{MI} gradually shifted to higher temperatures with decreasing film thickness as denoted by the arrows in Fig. 3(a). As shown in Fig. 3(b), $\rho(T)$ of the thicker films in metallic regime above T_{MI} can be expressed by a Fermi liquid model: $\rho = \rho_0 + AT^2$ where ρ_0 is the residual resistivity and A is the temperature coefficient of resistivity representing the inelastic scattering strength between electrons. The value of A was estimated to be in the order of $10^{-9} \Omega\text{-cmK}^{-2}$, consistent with a strongly correlated electron system.¹³ On the other hand, a non-Fermi liquid description of the resistivity ($\rho \propto T^{1.5}$) for bulk $\text{La}_{1-x}\text{Sr}_x\text{VO}_3$ was observed at the critical boundary between an AFM insulator and paramagnetic metal due to the AFM spin fluctuations.^{5,7,8}

Below T_{MI} (i.e., in the insulating region), the resistivity of the LSVO films was scaled with a Mott variable range hopping (VRH) model (i.e., $\ln\rho \sim T^{-1/4}$), which suggests that Anderson localization due to disorder caused by the random distribution of Sr^{+2} ions on the La^{+3} sites is responsible for the resistivity upturn seen at low temperatures below T_{MI} . The shift of T_{MI} to higher temperature with decreasing thickness implies that the critical disorder strength for

Anderson MIT gradually increases with decreasing film thickness and hence the stabilization of the insulating state is enhanced with decreasing film thickness. We also evaluated the disorder of the films from the residual resistivity, ρ_0 . The randomness of a system is characterized by the disorder parameter $k_F\ell$, the product of Fermi wave vector (k_F) and elastic mean free path (ℓ).¹⁴

The disorder parameter $k_F\ell$ is related to the residual sheet resistance, R_0 by the relation, $1/R_0 = (e^2/hR_0)k_F\ell$, where e and h are the electronic charge and Plank's constant, respectively. We obtained the values of $k_F\ell = 3.24, 2.42, 1.7$ and 1.44 for films with 25, 13, 10 and 8 uc thicknesses, respectively. This result suggests that the system disorder increases and approaches to the Ioffe-Regel limit ($k_F\ell \sim 1$) causing Anderson localization as the thickness is reduced, while the disorder parameters of the metallic films are above the Ioffe-Regel limit.

Figure 4 demonstrates the $O1s$ XAS spectra for the LSVO films. We have used normal (photon polarization parallel to film surface) and grazing incidences of the x-ray beam. The $O1s$ -edge XAS spectra display several features. The prominent doublet feature in the energy range of 526 to 528 eV and 529 to 531 eV are assigned to the $V3d t_{2g}$ and $V 3d e_g$ bands, respectively, and separated by ~ 2 eV due to crystal field splitting.¹⁵ The $V 3d e_g$ band overlaps with the La $5d$ and Sr $3d$ bands in the energy range from 529 to 536 eV. The qualitative features and positions of $V 3d t_{2g}$ peaks remained unchanged with decreasing film thickness from 25 to 8 uc (metallic films) and were similar for grazing and normal incidences. However, further reduction of the thickness to 5 uc (insulating phase), the intensity of the $V 3d t_{2g}$ band peak decreased significantly and $V 3d t_{2g}$ peaks was split into two peaks separated by ~ 0.8 eV (see lower inset of Fig. 4(b)). The splitting of the $V 3d t_{2g}$ band peak is more prominent in normal than grazing incidence (upper

inset of Fig. 4). A similar signature of d band splitting across the MIT was observed by Koethe *et al.* and Croft *et al.* in TMOs (VO_2) and sulfides (CuIr_2S_4).^{16,17} This result indicates that the occupation of $V3d$ orbitals is nearly isotropic in the metallic films and becomes anisotropic in insulating phase (i.e., preferential occupation in out-of-plane d_{yz} and d_{xz} orbitals). It is important to note that such changes in the d -orbital occupations across the MIT can be achieved only if the electron-electron correlation is strong enough to bring this narrow band system close to the Mott regime.¹⁸ It has been shown that electron correlation is significantly enhanced in the ultrathin limit (low dimension) and opens the Mott-Hubbard gap at the Fermi level to drive a correlated metallic system into the insulating state.⁹ Hence, the observed $V3d t_{2g}$ band splitting in the low dimensional LSVO films occurs only due to strong electron-electron correlation and the $V 3d t_{2g}$ band splitting gives rise to opening a gap at the Fermi level which possibly drives the formation of the insulating state in the 5 uc thick LSVO film. The $V2p$ spectra (not shown here) indicates that the V^{4+} concentrations of all films were above the nominal value (25%) of Sr doping, which can be attributed to surface oxidation or interface effects between the LSVO film and the LAO capping layer.^{19,20} Interestingly, the intensity of the V^{4+} features decreases progressively with decreasing film thickness. The decrease in V^{4+} ion concentration in the thinner films gives rise to the increase of disorder strength since the effective shielding of random impurity (Sr^{2+}) potential is diminished by the reduced charge carrier of the V^{4+} ion. This behavior is consistent with the change in the calculated disorder parameter, $k_F\ell$, with thickness.

In summary, we have shown that LSVO films, which are correlated metals in a bulk, undergo a MIT for thicknesses between 8uc to 5uc. The observed MIT is attributed to early onset of electron-electron correlation, i.e., bandwidth narrowing driven by the splitting of $V 3d t_{2g}$ band in low dimensional structures as well as Anderson localization represented by the disorder

parameter approaching to the Ioffe-Regel limit. The metallic films also exhibit MIT (resistivity upturn) at a thickness-dependent characteristic temperature during cooling, which is attributed to the Anderson localization.

This work is supported by the Basic Science Research Program through National Research Foundation of Korea (2009-0092809), the Director, Office of Science, Office of Basic Energy Sciences, of the U.S. Department of Energy (DE-AC02-05CH11231), and National Science Foundation (DMR 0747896).

This document was prepared as an account of work sponsored by the United States Government. While this document is believed to contain correct information, neither the United States Government nor any agency thereof, nor the Regents of the University of California, nor any of their employees, makes any warranty, express or implied, or assumes any legal responsibility for the accuracy, completeness, or usefulness of any information, apparatus, product, or process disclosed, or represents that its use would not infringe privately owned rights. Reference herein to any specific commercial product, process, or service by its trade name, trademark, manufacturer, or otherwise, does not necessarily constitute or imply its endorsement, recommendation, or favoring by the United States Government or any agency thereof, or the Regents of the University of California. The views and opinions of authors expressed herein do not necessarily state or reflect those of the United States Government or any agency thereof or the Regents of the University of California.

References

- ¹ M. Imada, A. Fujimori, and Y. Tokura, *Rev. Mod. Phys.* **70**, 1039(1998).
- ² N. F. Mott, *Metal-Insulator Transitions* (Taylor and Francis, London, 1974).
- ³ P. W. Anderson, *Phys. Rev.* **109**, 1498 (1958).
- ⁴ K. Byczuk, W. Hofstetter, and D. Vollhardt, *Phys. Rev. Lett.* **102**, 146403 (2009).
- ⁵ M. Sayer, R. Chent, R. Fletcher and A. Mansingh, *J. Phys. C: Solid State Phys.* **8**, 2059 (1975).
- ⁶ F. Inaba, T. Arima, T. Ishikawa, T. Katsufuji, and T. Tokura, *Phys. Rev. B* **52**, R2221 (1995).
- ⁷ S. Miyasaka, T. Okuda, and Y. Tokura, *Phys. Rev. Lett.* **85**, 5388 (2000).
- ⁸ I. Chaitanya Lekshmi, A. Gayen, M.S. Hegde, *J. Phys. Chem. Solids.* **66**, 1647 (2005).
- ⁹ K. Yoshimatsu, T. Okabe, H. Kumigashira, S. Okamoto, S. Aizaki, A. Fujimori, and M. Oshima, *Phys. Rev. Lett.* **104**, 147601 (2010).
- ¹⁰ H. Wadati, Y. Hotta, M. Takizawa, A. Fujimori, T. Susaki, and H.Y. Hwang, *J. App. Phys.* **102**, 053707 (2007).
- ¹¹ Y. Ren, A. A. Nugroho, A. A. Menovsky, J. Stremper, U. Ru'tt, F. Iga, T. Takabatake, and C. W. Kimball, *Phys. Rev. B* **67**, 014107 (2003).
- ¹² S. J. May, J.-W. Kim, J. M. Rondinelli, E. Karapetrova, N. A. Spaldin, A. Bhattacharya, and P. J. Ryan, *Phys. Rev. B* **82**, 014110 (2010).
- ¹³ M. J. MacEachern, H. Dabkowska, J. D. Garrett, G. Amow, W Gong, G. Liu, and J. E. Greedan, *Chem. Mater.* **6**, 2092 (1994).
- ¹⁴ D. J. Thouless, *Phys. Rev. Lett.* **39**, 1167(1977)
- ¹⁵ R. J. O. Mossaneck, M. Abbate, P. T. Fonseca, A. Fujimori, H. Eisaki, S. Uchida, and Y. Tokura, *Phys. Rev. B* **80**, 195107 (2009).

- ¹⁶ T. C. Koethe, Z. Hu, M. W. Haverkort¹, C. Schüßler-Langeheine, F. Venturini, N. B. Brookes, O. Tjernberg, W. Reichelt, H. H. Hsieh, H.-J. Lin, C. T. Chen, and L. H. Tjeng, *Phys. Rev. Lett.* **97**, 116402 (2006).
- ¹⁷ M. Croft, W. Caliebe, H. Woo, T. A. Tyson, D. Sills, Y. S. Hor, S-W. Cheong, V. Kiryukhin, and S-J. Oh, *Phys. Rev. B* **67**, 201102 (2003).
- ¹⁸ M. W. Haverkort, Z. Hu, A. Tanaka, W. Reichelt, S. V. Streltsov, M. A. Korotin, V. I. Anisimov, H. H. Hsieh, H.-J. Lin, C. T. Chen, D. I. Khomskii, and L. H. Tjeng, *Phys. Rev. Lett.* **95**, 196404 (2005).
- ¹⁹ H. Wadati, D. G. Hawthorn, J. Geck, T. Z. Regier, R. I. R. Blyth, T. Higuchi, Y. Hotta, Y. Hikita, H. Y. Hwang, and G. A. Sawatzky, *Appl. Phys. Lett.* **95**, 023115 (2009).
- ²⁰ M. Takizawa, Y. Hotta, T. Susaki, Y. Ishida, H. Wadati, Y. Takata, K. Horiba, M. Matsunami, S. Shin, M. Yabashi, K. Tamasaku, Y. Nishino, T. Ishikawa, A. Fujimori, and H. Y. Hwang, *Phys. Rev. Lett.* **102**, 236401 (2009).

Figure captions

Figure 1. Typical RHEED intensity oscillations during deposition for LSVO films with different thickness. The AFM topography image of LSVO films with 8 uc thickness is shown in the inset.

Figure 2. (a) XRD patterns (2θ - ω scans) for LSVO films with different thickness, (b) the variation of the c-axis lattice parameter with thickness and (c) the reciprocal space mapping for LSVO film with 25 uc thickness.

Figure 3. (a) Temperature-dependent electrical resistivity of LSVO films with different thickness. The arrows indicate a thickness dependent characteristic temperature (T_{MI}), and (b) resistivity vs. T^2 using the Fermi liquid model in the metallic region for films with 8-25 uc thickness.

Figure 4. O1s edge XAS taken at normal incidence for different film thickness. Details of the V $3d t_{2g}$ band for films with 5 and 8 uc thickness taken at normal (lower inset) and grazing (upper inset) incidence.

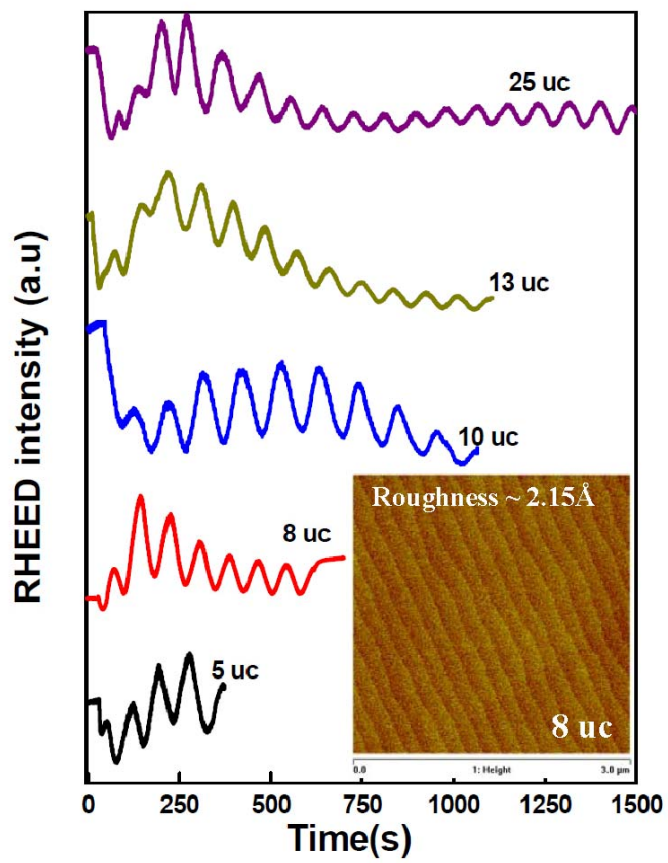


Figure 1

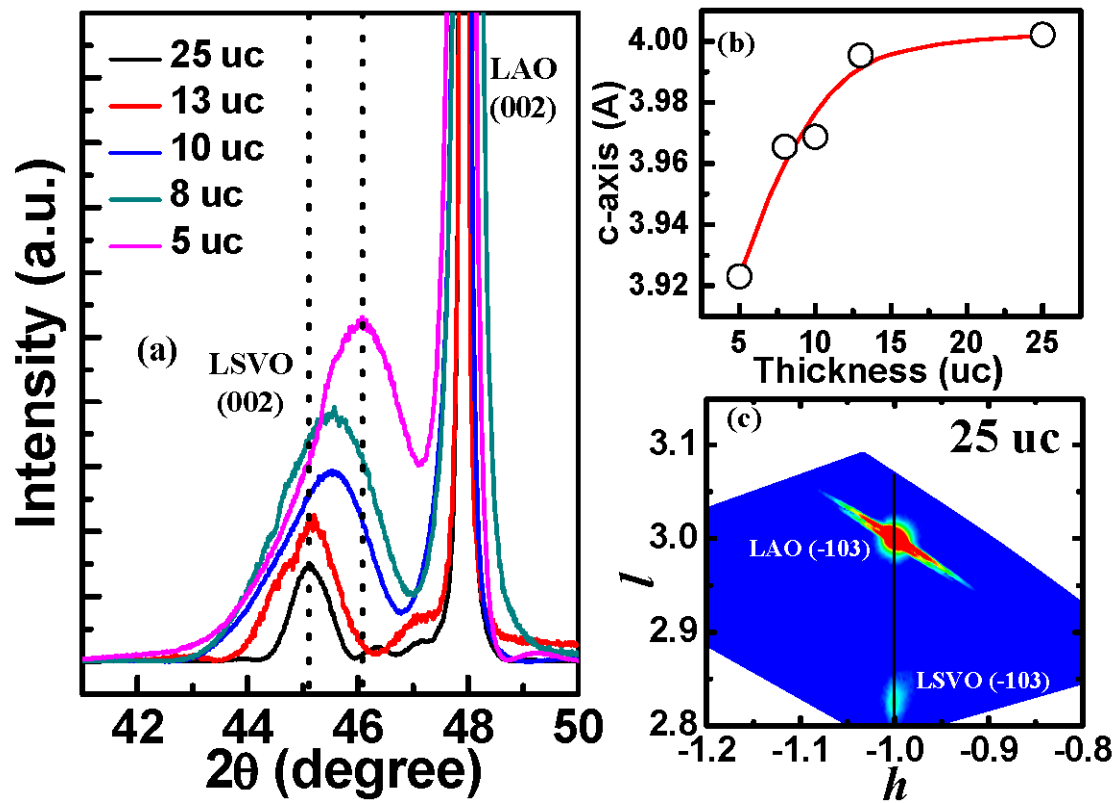


Figure 2

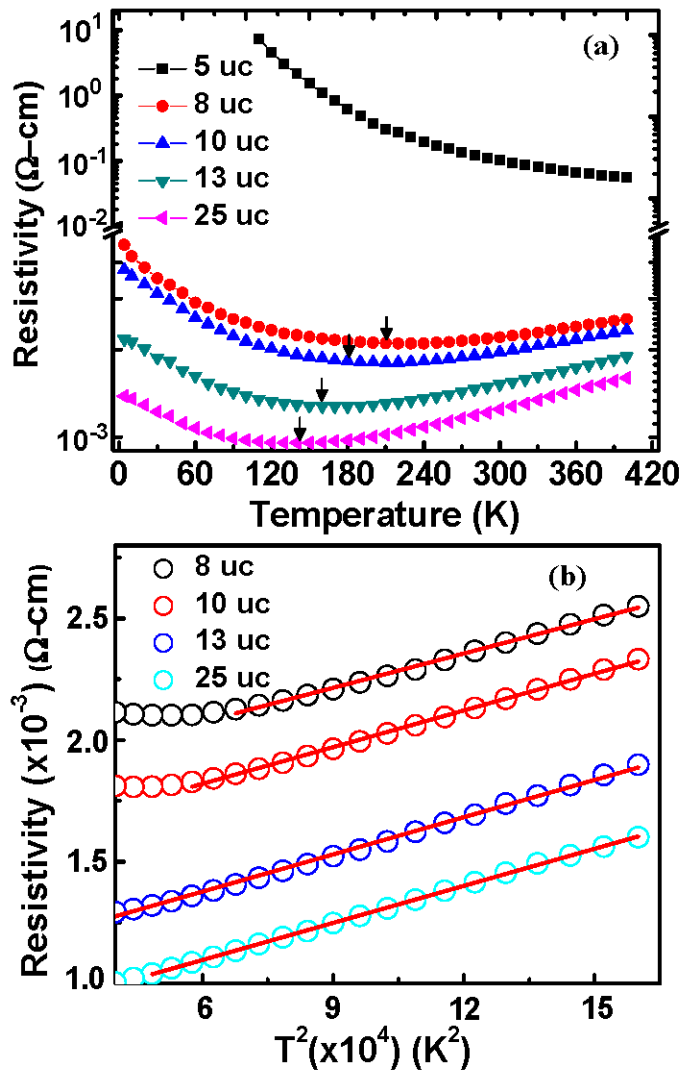


Figure 3

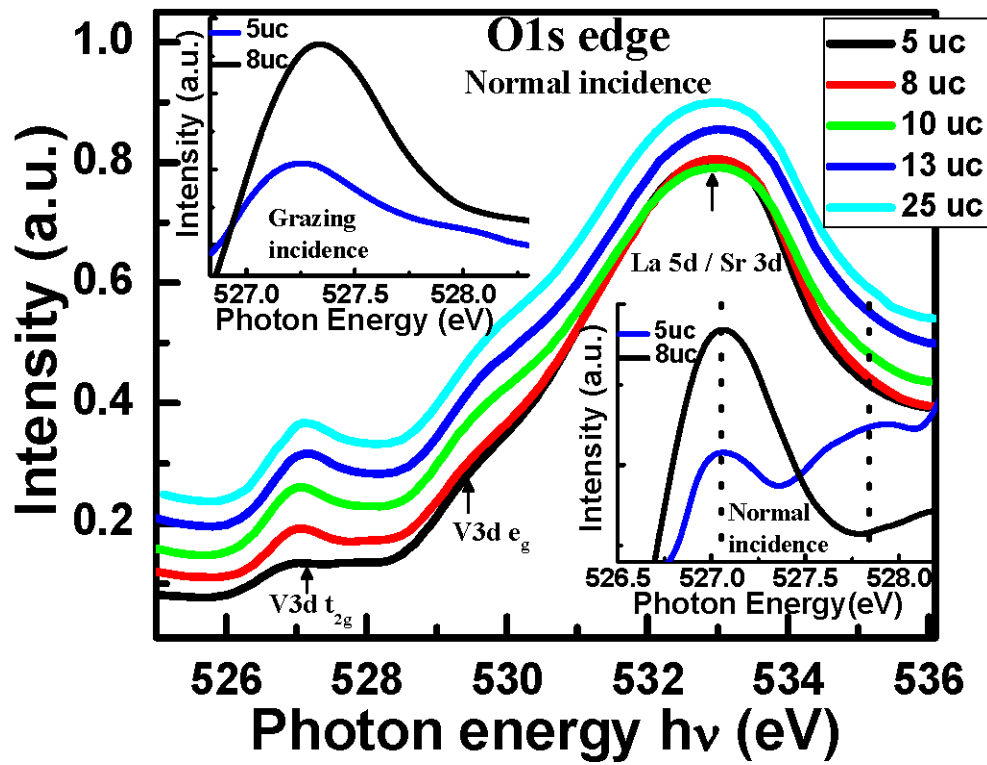


Figure 4